

An acceptor in a quantum dot

This article has been downloaded from IOPscience. Please scroll down to see the full text article.

1999 J. Phys.: Condens. Matter 11 6217

(<http://iopscience.iop.org/0953-8984/11/32/313>)

[The Table of Contents](#) and [more related content](#) is available

Download details:

IP Address: 129.8.242.67

The article was downloaded on 30/03/2009 at 11:20

Please note that [terms and conditions](#) apply.

An acceptor in a quantum dot

P Janiszewski and M Suffczyński

Institute of Physics, Polish Academy of Sciences, 02-668 Warsaw, Poland

Received 16 November 1998, in final form 30 March 1999

Abstract. Energy levels and oscillator strengths for transitions between the lowest states of an acceptor in a semiconductor quantum dot with a finite potential barrier have been computed in the effective-mass approximation, with the valence-band degeneracy in cubic semiconductors taken into account in the spherical approximation. Variational envelope functions have to satisfy the appropriate boundary conditions to ensure the hermiticity of the Hamiltonian matrix. In typical cubic semiconductors the acceptor optical transition energies and oscillator strengths are found to have enhanced values, larger by one order of magnitude than those in the bulk, in the dots of radius approximating in value to the diameter of the acceptor ground-state envelope.

1. Introduction

Studies of zero-dimensional semiconductor quantum dots may be aided by systematic quantum mechanical calculations of the electronic properties of these low-dimensional structures which are now being constructed with increasingly better specified parameters. The electronic structure of quantum dots is investigated [1–3] by various methods. An impurity in a quantum well, quantum wire, or quantum dot has an energy spectrum determined not only by the potential of the impurity centre but also by the confining potential of the barrier. A carrier bound to an impurity atom located in a quantum dot of radius comparable to the envelope function extent has states modified considerably from those in the bulk. The description of the impurity states in a quantum dot with a low potential barrier can moreover serve further as a model for the carrier bound states due to the fluctuation-type imperfections in the crystal lattice.

2. The effective-mass equation for an acceptor in a quantum dot

We consider an impurity located at the centre of a spherical quantum dot of radius R of semiconductor ‘I’, embedded in a semiconductor ‘E’. An impurity-bound carrier in this system is described in the effective-mass approximation by solution of the Schrödinger-type equation

$$\mathcal{H}\Phi = E\Phi \quad (1)$$

with the Hamiltonian

$$\mathcal{H} = \begin{cases} \mathcal{H}^I + V_C^I - V_B & r < R \\ \mathcal{H}^E + V_C^E & r > R \end{cases} \quad (2)$$

and an envelope function

$$\Phi(\vec{r}) = \begin{cases} \Phi^I(\vec{r}) & r < R \\ \Phi^E(\vec{r}) & r > R \end{cases} \quad (3)$$

where \mathcal{H}^I and \mathcal{H}^E are the effective-mass kinetic energy operators of the carrier inside and outside of the dot, respectively. The V_B is the height of the potential barrier between the respective valence bands in semiconductors I and E, and

$$V_C^{I,E} = -Ze^2/(\varepsilon^{I,E}r) \quad (4)$$

(with $Z = 1$) is the Coulomb potential energy. The static dielectric constant is $\varepsilon^{I,E}$ inside and outside of the dot, respectively. The dielectric mismatch has been taken into account by various approximations [4–8].

In a cubic semiconductors, in the limit of large spin–orbit splitting in the valence band, the hole in the upper subband Γ_8 can be described as a particle with spin $J = 3/2$, due to the periodic part of the band-edge wave function. The hole kinetic energy is given by the Luttinger Hamiltonian [9, 10], and the anisotropic effective masses are described by the Luttinger parameters $\gamma_1^{I,E}$, $\gamma_2^{I,E}$, $\gamma_3^{I,E}$. We neglect the warping of the valence band, i.e. we restrict the calculations to the spherical approximation [2, 11–16], and replace $\gamma_2^{I,E}$ and $\gamma_3^{I,E}$ by $\bar{\gamma}^{I,E} = (2\gamma_2^{I,E} + 3\gamma_3^{I,E})/5\gamma_1^{I,E}$. Accordingly, the parameter $\mu^{I,E}$ which describes the strength of the spherical part of the spin–orbit interaction is

$$\mu^{I,E} = 2\bar{\gamma}^{I,E}/\gamma_1^{I,E}. \quad (5)$$

The hole kinetic Hamiltonians \mathcal{H}^I and \mathcal{H}^E can be represented with use of the irreducible tensors $P^{(2)}$ and $J^{(2)}$, composed of the momentum operator $\vec{p} = -i\hbar\vec{\nabla}$ and the spin angular momentum operator \vec{J} of the hole, respectively:

$$\mathcal{H}^{I,E} = \frac{\gamma_1^{I,E}}{2m_0} [\vec{p}^2 - \mu^{I,E}(P^{(2)} \cdot J^{(2)})] \quad (6)$$

Baldereschi and Lipari [9, 10] defined $P^{(2)}$ with a prefactor, $P^{(2)} = 3(P^{(1)} \otimes P^{(1)})$; we follow monograph [17] in defining the irreducible tensor operators, and have no prefactor in the spin–orbit coupling term $P^{(2)} \cdot J^{(2)}$, as described in appendix A. The effective Bohr radius $a_0 = \hbar^2\varepsilon_0/m_0e^2$ and the effective Rydberg $\text{Ryd} = m_0e^4/2\hbar^2\varepsilon_0^2$, with the free-electron mass m_0 and $\varepsilon_0 = \varepsilon^I$, will be units of length and energy, respectively.

The hole from the upper valence subband, bound to a spherically symmetric potential, has, besides the spin \vec{J} , an orbital angular momentum \vec{L} . Since the total angular momentum $\vec{F} = \vec{L} + \vec{J}$ commutes with both Hamiltonians \mathcal{H}^I and \mathcal{H}^E , and the spin–orbit term couples states with $|L' - L| = 0, 2$, the hole envelope functions can be written in the form [9, 11, 18]

$$\begin{aligned} \Phi(S_{3/2}) &= f_{01}(r)|0, 3/2, 3/2, F_z\rangle + f_{02}(r)|2, 3/2, 3/2, F_z\rangle \\ \Phi(P_{1/2}) &= f_{11}(r)|1, 3/2, 1/2, F_z\rangle \\ \Phi(P_{3/2}) &= f_{21}(r)|1, 3/2, 3/2, F_z\rangle + f_{22}(r)|3, 3/2, 3/2, F_z\rangle \\ \Phi(P_{5/2}) &= f_{31}(r)|1, 3/2, 5/2, F_z\rangle + f_{32}(r)|3, 3/2, 5/2, F_z\rangle \\ \Phi(D_{1/2}) &= f_{41}(r)|2, 3/2, 1/2, F_z\rangle \\ \Phi(D_{5/2}) &= f_{51}(r)|2, 3/2, 5/2, F_z\rangle + f_{52}(r)|4, 3/2, 5/2, F_z\rangle \\ \Phi(D_{7/2}) &= f_{61}(r)|2, 3/2, 7/2, F_z\rangle + f_{62}(r)|4, 3/2, 7/2, F_z\rangle \end{aligned} \quad (7)$$

where the kets $|L, J, F, F_z\rangle$ are eigenfunctions of the total angular momentum F in the L – J coupling scheme, and the four figures in the ket represent the eigenvalues of the operators L^2 , J^2 , F^2 , and F_z , respectively. We write the simplified index (a) instead of a part, or the whole set, of quantum numbers, and omit this index when an envelope function of only one state is considered. The index i ($=1, 2$) labels the two components of the envelope. The components of the radial functions, $f_1(r)$ and $f_2(r)$, have to satisfy the set of differential

equations [9, 11, 18–20]

$$\begin{bmatrix} H_{11} - E & H_{12} \\ H_{21} & H_{22} - E \end{bmatrix} \begin{bmatrix} f_1(r) \\ f_2(r) \end{bmatrix} = 0 \tag{8}$$

where

$$\begin{aligned} H_{11} &= -\gamma_1(1 + C_1) \left[\frac{d^2}{dr^2} + \frac{2}{r} \frac{d}{dr} - \frac{L(L+1)}{r^2} \right] + V(r) \\ H_{12} &= \gamma_1 C_2 \left[\frac{d^2}{dr^2} + \frac{2L+5}{r} \frac{d}{dr} + \frac{(L+1)(L+3)}{r^2} \right] \\ H_{21} &= \gamma_1 C_2 \left[\frac{d^2}{dr^2} - \frac{2L+1}{r} \frac{d}{dr} + \frac{L(L+2)}{r^2} \right] \\ H_{22} &= -\gamma_1(1 - C_1) \left[\frac{d^2}{dr^2} + \frac{2}{r} \frac{d}{dr} - \frac{(L+2)(L+3)}{r^2} \right] + V(r) \end{aligned} \tag{9}$$

with the spherically symmetric potential energy $V(r) = V_C - V_B$. The coefficients C_1/μ for the states of equation (7) are listed [9, 11, 18, 20] in table 1, and $C_2 = (\mu^2 - C_1^2)^{1/2}$.

Table 1. Coefficients in the hole Hamiltonian of equation (9).

	S _{3/2}	P _{1/2}	P _{3/2}	P _{5/2}	D _{1/2}	D _{5/2}	D _{7/2}
C_1/μ	0	1	-4/5	1/5	1	-5/7	2/7

3. Boundary conditions

To satisfy the requirements of quantum mechanics, in particular to secure the real eigenvalues of energy, the hermiticity of Hamiltonian (2) has to be assured by a proper choice of boundary conditions, i.e. the behaviour of Φ^I at $r \rightarrow 0$ and of Φ^E at $r \rightarrow \infty$, and, in a spatially confined system, an appropriate relation between functions Φ^I and Φ^E at the system sharp boundary $r = R$. The former conditions are that Φ^I has to be non-singular at $r = 0$, and Φ^E has to decay exponentially with r when $r \rightarrow \infty$; they ensure the existence of the normalization integral in a bound system. The relation between functions Φ^I and Φ^E is crucial for a system with a potential barrier, and has to be established [21–24] according to the particular form [25, 26] of \mathcal{H}^I and \mathcal{H}^E .

The general definition of a Hermitian conjugate \mathcal{O}^\dagger of an operator \mathcal{O} ,

$$\langle \Psi | \mathcal{O} \Phi \rangle = \langle \mathcal{O}^\dagger \Psi | \Phi \rangle \tag{10}$$

where Φ and Ψ are any functions from the space of states, is used for computation of \mathcal{H}^\dagger for \mathcal{H} given by equations (2) and (6) in the space of envelope functions Φ and Ψ of the form of equation (3). By using the identity

$$P^{(2)} \cdot J^{(2)} = -\nabla^{(2)} \cdot J^{(2)} = \sqrt{5/3} \nabla_1 \cdot (\nabla_1 \otimes J^{(2)})_1 \tag{11}$$

and Green’s theorem, we find that $\mathcal{H} = \mathcal{H}^\dagger$ when the integrals over the full solid angle with the envelope functions (3) are equal on both sides of the boundary at $r = R$:

$$\begin{aligned} &\gamma_1^I \int (\langle \Psi^I | (\vec{n} \cdot \vec{\nabla}) | \Phi^I \rangle - \mu^I \langle \Psi^I | (n_1 \otimes \nabla_1)_2 \cdot J^{(2)} | \Phi^I \rangle) d\Omega \\ &= \gamma_1^E \int (\langle \Psi^E | (\vec{n} \cdot \vec{\nabla}) | \Phi^E \rangle - \mu^E \langle \Psi^E | (n_1 \otimes \nabla_1)_2 \cdot J^{(2)} | \Phi^E \rangle) d\Omega. \end{aligned} \tag{12}$$

To fulfil equation (12), the radial functions \bar{f} , at the dot boundary, $r = R$, have to be continuous, $\bar{f}^I = \bar{f}^E$, and the radial derivatives have to satisfy

$$d\bar{f}^I/dr = (A^I)^{-1}[A^E d\bar{f}^E/dr + (B^E - B^I)\bar{f}^E/R] \quad (13)$$

where the functions f_{ai} are written as two-component vectors \bar{f} , and the 2×2 matrices $A^{I,E}$ and $B^{I,E}$ are defined in appendix A.

4. Calculation of the envelopes

To find a variational solution of equation (8) we used an expansion of the radial functions $f_{ai}(r)$ in a series of N exponential functions $c_{ain} \exp(-q^n r/R_{\text{amax}})$ with $n = 1, 2, \dots, N$. The values of the radius R_{amax} and of the scale factor q were found by trial and error to minimize the energy eigenvalue E . The value of the scale parameter q was, in most cases, equal to 2; its smallest value used was 1.67, the largest 2.2. The number N of basis exponential functions was varied, according to the needs of a particular calculated state, between 5 and 20 for the envelope part inside the dot, and between 3 and 10 outside of the dot. The two conditions for hermiticity of the Hamiltonian: continuity of the envelope and equation (13), allow one to eliminate two from the N components of each envelope, and thus to reduce the dimension of the secular determinant from $2N$ to $2(N - 2)$. For the component functions $f_{ai}(r)$ with $L > 0$, one of the coefficients c_{ain} was adjusted so as to make $f_{ai}(0) = 0$. We have computed the lowest and the first excited energy levels for the states specified in table 1.

We also calculated the energy levels in a spherical dot with a potential barrier of infinite height, using finite sets [11–13] of the basis radial functions: $[2/R]^{1/2} r^{-1} \sin(n\pi r/R)$, and also $\exp(-\alpha_n r) \cos(\pi r/2R)$, with integer $n < N$. The hole energy levels, calculated without the Coulomb potential, recover the closed-form results obtained with the analytical use of spherical Bessel functions [8, 12, 13]. To check our calculated envelope functions, at least for the particular case of $\mu = 0$, we have computed with them the expectation values of the r -coordinate, which determine the dipole oscillator strength, and compared them with the values of analytical expressions for hydrogen atom. The values agreed within an accuracy of 10^{-3} or better. Our computed values of the oscillator strengths agreed with the corresponding values calculated with exact analytical acceptor envelopes [20] to at least two digits.

5. Energy levels

We consider quantum dots in semiconductors with cubic zinc-blende crystallographic structure. Examples of the computed energy levels for the on-centre acceptor are presented in figure 1, in units of the effective Rydberg $\text{Ryd}_{\text{HH}} = \text{Ryd} \times m_{\text{HH}}/m_0$ of the heavy hole, as function of the dot radius, expressed in units of the effective Bohr radius $a_{0\text{HH}} = a_0 \times m_0/m_{\text{HH}}$ of the heavy hole with the effective-mass value of the inside of the dot:

$$m_{\text{HH}} = m_0/[\gamma_1^I(1 - \mu^I)] = m_0/(\gamma_1^I - 2\bar{\gamma}^I).$$

For the GaAs quantum dot embedded in a $\text{Ga}_{1-x}\text{Al}_x\text{As}$ matrix we adopted [27, 28] the following parameters: for GaAs, $\gamma_1^I = 6.79$, $\bar{\gamma}^I = 2.378$, $\varepsilon_0 = 12.56$; for AlAs, $\gamma_1^E = 3.79$, $\bar{\gamma}^E = 1.329$, $\varepsilon^E = 10.06$; and for $\text{Ga}_{1-x}\text{Al}_x\text{As}$, the values of the parameters obtained by linear interpolation [27]. The band-gap difference [6] is given by $\Delta E_g = 1247$ meV, and we assumed [28, 29] the ratio of the valence-band offset to the band-gap difference $\Delta E_v/\Delta E_g = 0.35$, so the potential barrier height $V_B = 0.35 \times 1247 \times x$ meV. For the GaAs quantum dot in a ZnSe matrix we adopted: $\gamma_1^E = 4.212$, $\bar{\gamma}^E = 1.465$, $\varepsilon^E = 9.1$, outside of the dot [28, 30–33]. In GaAs, $\text{Ryd}_{\text{HH}} = 42.4$ meV and $a_{0\text{HH}} = 13.5$ Å. For the CdTe

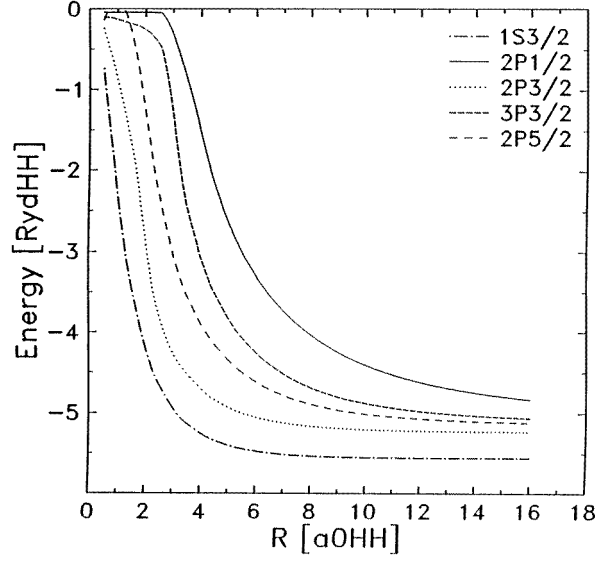


Figure 1. The computed energy levels of the on-centre acceptor, in units of the effective Rydberg Ryd_{HH} of the heavy hole, as functions of the dot radius R , expressed in units of the effective Bohr radius $a_{0\text{HH}}$ of the heavy hole, with $\gamma_1^{\text{I}} = \gamma_1^{\text{E}}$ and $\mu^{\text{I}} = \mu^{\text{E}} = 0.7$. The potential barrier height is $V_{\text{B}} = 5 \text{ Ryd}_{\text{HH}}$.

quantum dot in cubic $\text{Cd}_{1-x}\text{Mn}_x\text{Te}$ we have taken $\varepsilon_0 = 9.7$, and $\gamma_1 = 5.5$, $\bar{\gamma} = 2.0$, inside and outside of the dot [34, 35]. The computed low energy levels of an acceptor at the centre of a GaAs spherical quantum dot embedded in $\text{Ga}_{1-x}\text{Al}_x\text{As}$ with $x = 0.4$, corresponding [6, 29] to the potential barrier height $V_{\text{B}} = 175 \text{ meV}$, are shown in figure 2 as functions of the dot radius R between 10 \AA and 200 \AA . Figure 3 shows the computed low energy levels of an acceptor at the centre of the GaAs quantum dot in ZnSe where we adopted [29–32] the barrier height $V_{\text{B}} = 350 \text{ meV}$. Figure 4 shows the computed low energy levels of an acceptor at the centre of the CdTe in a $\text{Cd}_{1-x}\text{Mn}_x\text{Te}$ quantum dot with $x = 0.24$, corresponding [29, 35, 36] to $V_{\text{B}} = 25 \text{ meV}$.

6. Optical transitions

With the calculated energies and envelope functions for the acceptor states, we have computed the oscillator strengths f_{ab} of optical dipole transitions between the acceptor initial state Ψ_a and an excited state Φ_b with the corresponding energies E_a and E_b , respectively [8, 14, 21, 37].

The expression for the f_{ab} , described in appendix B, is obtained by averaging over the degenerate states F_{0z} of the initial (a) = $(n_0, L_0, 3/2, F_0, F_{0z})$ level, and summing over the states F_z of the final (b) = $(n, L, 3/2, F, F_z)$ level:

$$f_{ab} = \frac{2m_0}{\hbar^2 \gamma_1^R} (E_b - E_a) \frac{1}{2F_0 + 1} \sum_{F_{0z}, F_z} |\langle \Psi_{a, F_{0z}}^{\text{I}} | z | \Phi_{b, F_z}^{\text{I}} \rangle + \langle \Psi_{a, F_{0z}}^{\text{E}} | z | \Phi_{b, F_z}^{\text{E}} \rangle|^2. \quad (14)$$

Figure 5(a) shows the computed photon energies, expressed in units of Ryd_{HH} , of transitions from the ground state $1\text{S}_{3/2}$ to the lowest excited states, 2P and $3\text{P}_{3/2}$, of the on-centre acceptor in a quantum dot of radius R , expressed in units of $a_{0\text{HH}}$. Figure 5(b) shows the oscillator strengths of the $1\text{S}_{3/2} \rightarrow 2\text{P}$ and $\rightarrow 3\text{P}_{3/2}$ transitions for the on-centre acceptor

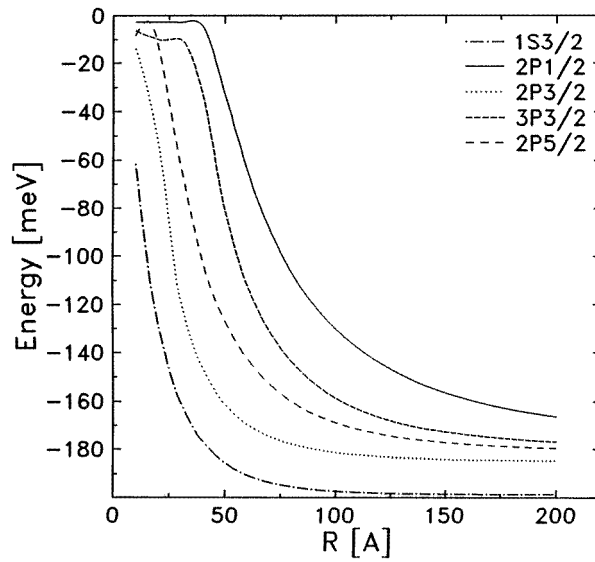


Figure 2. The low energy levels of an acceptor at the centre of the GaAs quantum dot in $\text{Ga}_{1-x}\text{Al}_x\text{As}$, with the potential barrier height $V_B = 175$ meV.

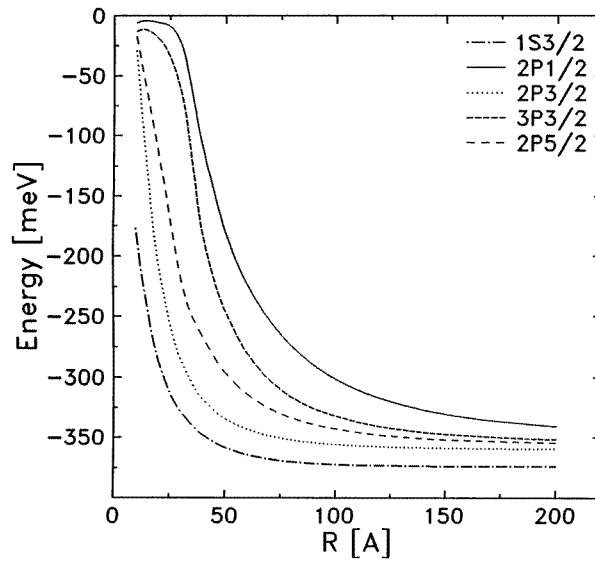


Figure 3. The low energy levels of an acceptor at the centre of the GaAs quantum dot in ZnSe, with the potential barrier height $V_B = 350$ meV.

in a quantum dot of radius R , expressed in units of $a_{0\text{HH}}$, with the potential barrier height $V_B = 5 \text{ Ryd}_{\text{HH}}$.

For a GaAs quantum dot in $\text{Ga}_{1-x}\text{Al}_x\text{As}$ with $x = 0.4$, corresponding to the potential barrier height $V_B = 175$ meV, the photon energies and the oscillator strengths of the $1S_{3/2} \rightarrow 2P$ and $\rightarrow 3P_{3/2}$ transitions, for the on-centre acceptor, are shown in figures 6(a)

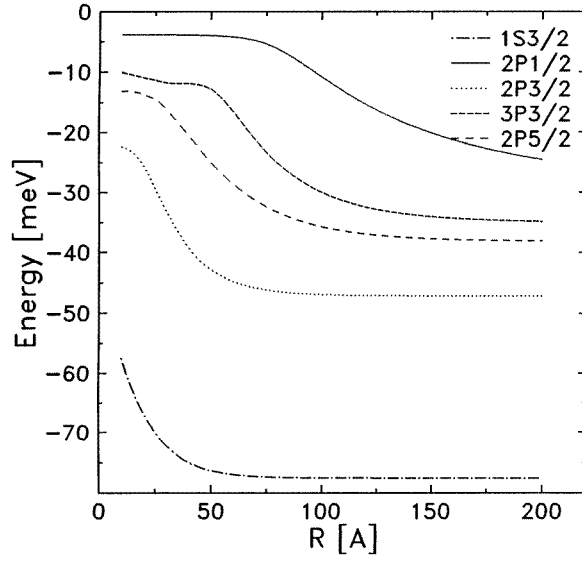


Figure 4. The low energy levels of an acceptor at the centre of the CdTe quantum dot in $\text{Cd}_{1-x}\text{Mn}_x\text{Te}$, with the potential barrier height $V_B = 25$ meV.

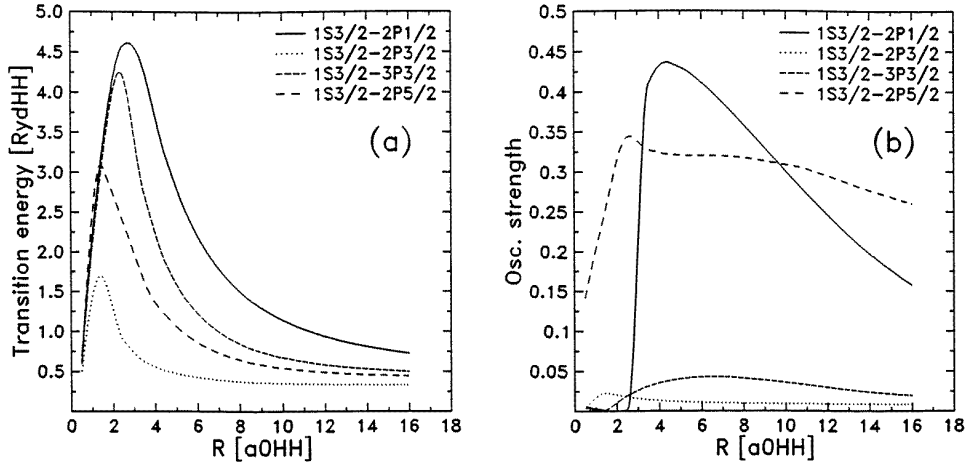


Figure 5. (a) Photon energies, expressed in units of Ryd_{HH} , of the $1\text{S}_{3/2} \rightarrow 2\text{P}$ and $\rightarrow 3\text{P}_{3/2}$ transitions for an acceptor at the centre of a quantum dot of radius R , expressed in units of $a_{0\text{HH}}$. (b) Oscillator strengths of the $1\text{S}_{3/2} \rightarrow 2\text{P}$ and $\rightarrow 3\text{P}_{3/2}$ transitions for the on-centre acceptor. The potential barrier height is $V_B = 5 \text{Ryd}_{\text{HH}}$.

and 6(b), respectively, as functions of the dot radius between $R = 10 \text{ \AA}$ and 200 \AA . In the $\text{GaAs}/\text{Ga}_{1-x}\text{Al}_x\text{As}$ quantum dot of radius between $2a_{0\text{HH}}$ and $4a_{0\text{HH}}$, the oscillator strength of the acceptor $1\text{S}_{3/2} \rightarrow 2\text{P}_{1/2}$ transition is larger than that in the bulk by one order of magnitude, and for the transition $1\text{S}_{3/2} \rightarrow 2\text{P}_{5/2}$ by a factor of about 1.6. For the on-centre acceptor in a GaAs quantum dot in ZnSe, with the adopted [29, 32] barrier height $V_B = 350$ meV, the photon energies and the oscillator strengths of the $1\text{S}_{3/2} \rightarrow 2\text{P}$ and $\rightarrow 3\text{P}_{3/2}$ transitions are

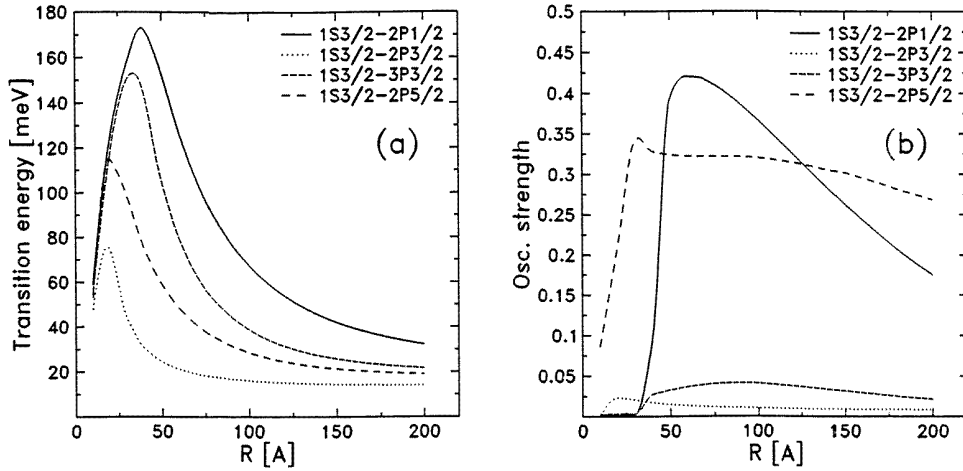


Figure 6. (a) Photon energies and (b) oscillator strengths of the $1S_{3/2} \rightarrow 2P$ and $\rightarrow 3P_{3/2}$ transitions for an acceptor at the centre of the GaAs quantum dot in $\text{Ga}_{1-x}\text{Al}_x\text{As}$, with the potential barrier height $V_B = 175$ meV.

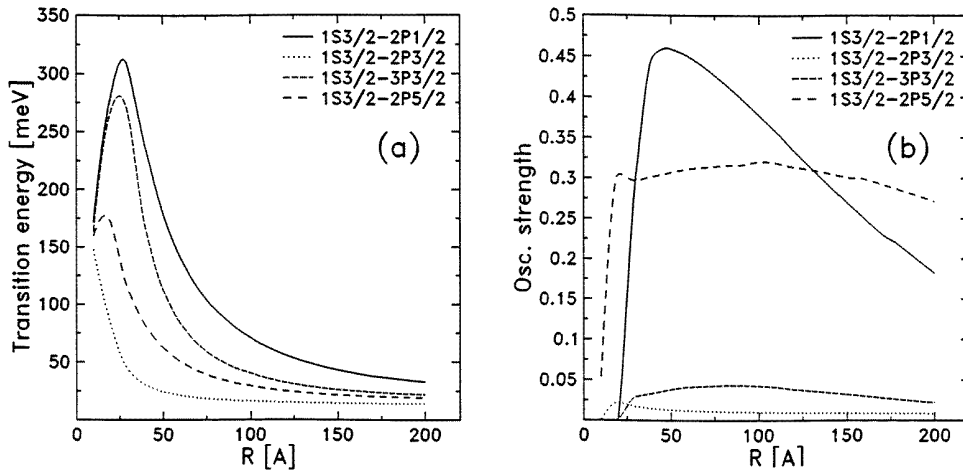


Figure 7. (a) Photon energies and (b) oscillator strengths of the $1S_{3/2} \rightarrow 2P$ and $\rightarrow 3P_{3/2}$ transitions for an acceptor at the centre of the GaAs quantum dot in ZnSe, with the potential barrier height $V_B = 350$ meV.

shown in figures 7(a) and 7(b), respectively. A large enhancement of the oscillator strength in the dot is seen for the $1S_{3/2} \rightarrow 2P_{1/2}$ transition and the $1S_{3/2} \rightarrow 2P_{5/2}$ transition. For the on-centre acceptor in a CdTe quantum dot [29, 35, 36] in $\text{Cd}_{1-x}\text{Mn}_x\text{Te}$ with $x = 0.24$, the photon energies and the oscillator strengths are shown in figures 8(a) and 8(b), respectively.

The oscillator strengths of transitions from the acceptor ground state $1S_{3/2}$ to the first excited states, $2P_{1/2}$ and $2P_{5/2}$, have remarkably large values [20, 37], sensitively dependent, at small dot radii, on the dot radius. At dot radii larger than $R = 2a_{0\text{HH}}$, the oscillator strengths for the on-centre acceptor in a quantum dot decrease rather slowly with increase of the dot radius. Thus the enhancement of the oscillator strengths will not be affected by the dispersion [3, 38]

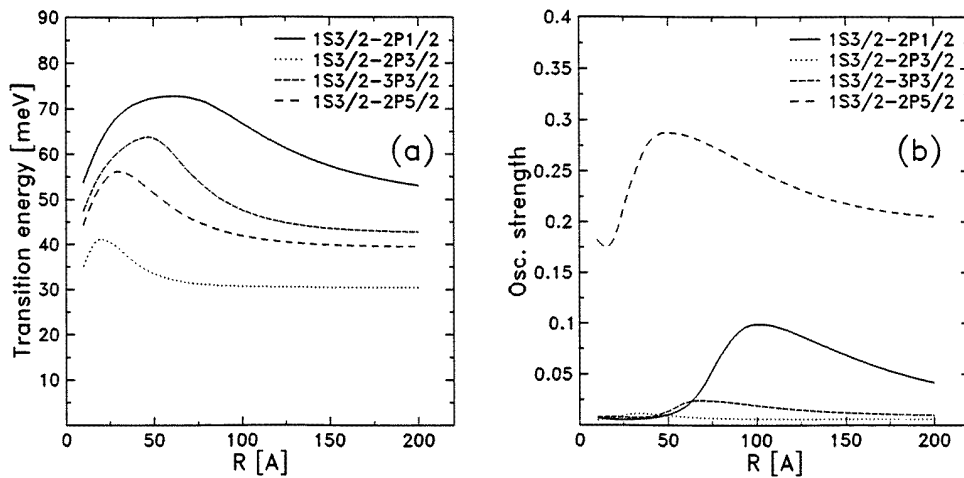


Figure 8. (a) Photon energies and (b) oscillator strengths of the $1S_{3/2} \rightarrow 2P$ and $\rightarrow 3P_{3/2}$ transitions for an acceptor at the centre of the CdTe quantum dot in $\text{Cd}_{1-x}\text{Mn}_x\text{Te}$, with the potential barrier height $V_B = 25$ meV.

of the dot radii between $R = 2a_{0\text{HH}}$ and $R = 4a_{0\text{HH}}$. On taking into account the dielectric mismatch, $\epsilon^E < \epsilon_0$, the computed transition energies increase, chiefly in the dots with radii of about one nanometre, by around 10%, and the oscillator strengths increase by around 1%. For the dots with larger radius this increase is smaller.

7. Concluding remarks

The low energy states of an acceptor at the centre of a quantum dot with a finite potential barrier, in cubic semiconductors with valence-band degeneracy, have been calculated in the effective-mass approximation. In the spherical approximation, the total angular momentum of the hole commutes with the Hamiltonian, and the use of the angular momentum eigenstates is convenient. Matching the acceptor multicomponent envelope functions in cubic semiconductors at the dot heterointerface ensures the hermiticity of the Hamiltonian, whose eigenvalues are the allowed energies of the acceptor states. If the dot radius is larger than the diameter of the acceptor ground-state envelope the energies of the transitions between the low acceptor states increase with decreasing dot size [6, 14, 39, 40]. The corresponding dipole oscillator strengths for transitions from the acceptor ground state to the first excited states, in a quantum dot of radius approximating to the diameter of the acceptor ground-state envelope, is enhanced by one order of magnitude in comparison with the value for the acceptor in the bulk, as for quantum wells and wires [6, 14, 40]. The enhancement is due to a favourable overlap of the excited and the ground-state envelope functions in the quantum dot of appropriate range of dot radius. The range is larger when the potential barrier is higher. The energies and the envelope functions in the quantum dot calculated in the effective-mass approximation recover closely those in the bulk at the dot radius one order of magnitude larger than the acceptor effective Bohr radius. For the dot radius one order of magnitude smaller than the acceptor Bohr radius, the effective-bond-orbital model [4, 41, 42] offers a rationally founded method which requires computations larger by several orders of magnitude.

Examples of the low energy levels of the on-centre acceptor in quantum dot, and of

the oscillator strengths, are presented here for quantum dots with finite potential barriers encountered in typical cubic semiconductors. The transitions between the electron and the hole states with non-zero angular momentum quantum numbers have been observed in cylindrical quantum dots by luminescence measurements, and the transition energies have been found to increase with decreasing dot size [39, 40, 43–46].

Appendix A

The gradient $\vec{\nabla}$ in equation (12) consists of partial derivatives with respect to the radial, r , and to the angular coordinates [17]:

$$\vec{\nabla} = \vec{n} \frac{\partial}{\partial r} + \frac{1}{r} \vec{\nabla}_\Omega \quad (\text{A.1})$$

with $\vec{n} = \vec{r}/r = \hat{n}_1 = n_{1(-1,0,1)}$. The tensorial products of the second rank

$$N_2 = (n_1 \otimes n_1)_2 \quad D_2 = (n_1 \otimes (\nabla_\Omega)_1)_2 \quad (\text{A.2})$$

appear in the second-rank tensor operator

$$(n_1 \otimes \nabla_1)_2 = (n_1 \otimes n_1)_2 \frac{\partial}{\partial r} + \frac{1}{r} (n_1 \otimes (\nabla_\Omega)_1)_2 = N_2 \frac{\partial}{\partial r} + \frac{1}{r} D_2. \quad (\text{A.3})$$

Integrals in equation (12) are extended over the full solid angle, and can be expressed with the use of the 2×2 matrices

$$\begin{aligned} A_{ij} &= \gamma_1 \langle L_i, 3/2, F, F_z | -1 + \mu (N_2 \cdot J^{(2)}) | L_j, 3/2, F, F_z \rangle \\ B_{ij} &= \mu \gamma_1 \langle L_i, 3/2, F, F_z | (D_2 \cdot J^{(2)}) | L_j, 3/2, F, F_z \rangle. \end{aligned} \quad (\text{A.4})$$

Matrix elements of the scalar product of the second-rank tensors \mathcal{O}_2 and $J^{(2)}$, dependent on the space and spin coordinates, respectively, are expressed [17] with the 6- j symbols

$$\begin{aligned} &\langle L', 3/2, F', F'_z | \mathcal{O}_2 \cdot J^{(2)} | L, 3/2, F, F_z \rangle \\ &= (-1)^{F+L+3/2} \delta_{FF'} \delta_{F_z F'_z} \left\{ \begin{matrix} L' & L & 2 \\ 3/2 & 3/2 & F \end{matrix} \right\} \langle L' || \mathcal{O}_2 || L \rangle \langle 3/2 || J^{(2)} || 3/2 \rangle \end{aligned} \quad (\text{A.5})$$

where $|L' - L| = 0, 2$. The reduced matrix elements connecting the angular momentum eigenstates are

$$\begin{aligned} \langle L+2 || N_2 || L \rangle &= [(L+1)(L+2)/(2L+3)]^{1/2} \\ \langle L-2 || N_2 || L \rangle &= [L(L-1)/(2L-1)]^{1/2} \\ \langle L || N_2 || L \rangle &= -\{2L(L+1)(2L+1)/[3(2L-1)(2L+3)]\}^{1/2} \\ \langle L+2 || D_2 || L \rangle &= -L[(L+1)(L+2)/(2L+3)]^{1/2} \\ \langle L-2 || D_2 || L \rangle &= (L+1)[L(L-1)/(2L-1)]^{1/2} \\ \langle L || D_2 || L \rangle &= -\{3L(L+1)(2L+1)/[2(2L-1)(2L+3)]\}^{1/2} \\ \langle 3/2 || J^{(2)} || 3/2 \rangle &= \sqrt{30}. \end{aligned} \quad (\text{A.6})$$

The radial functions $\tilde{f}(r)$ of the envelope Φ , the radial functions $\tilde{g}(r)$ of Ψ , in equation (12), and the matrices A and B of equation (A.4), depend on the respective values of the Luttinger parameters in semiconductors I, E. The hermiticity of the Hamiltonian matrix requires, at the dot boundary, $r = R$, besides the equalities

$$\tilde{f}^I = \tilde{f}^E \quad \tilde{g}^I = \tilde{g}^E \quad (\text{A.7})$$

also the equality of the products

$$\tilde{g}^I \left[A^I \frac{d\tilde{f}^I}{dr} + B^I \frac{\tilde{f}^I}{R} \right] = \tilde{g}^E \left[A^E \frac{d\tilde{f}^E}{dr} + B^E \frac{\tilde{f}^E}{R} \right]. \quad (\text{A.8})$$

Appendix B

In the space inside (I) and outside of (E) the quantum dot, the values of the Luttinger parameter γ_1 are γ_1^I and γ_1^E , and the corresponding parts of the envelope function are Φ_a^I and Φ_a^E , respectively. The normalization integral of the envelope functions, and the matrix element of the dipole moment, consist of contributions from the space inside (I)

$$c_a^I = \langle \Phi_a^I | \Phi_a^I \rangle = \int d\Omega \int_0^R |\Phi_a^I|^2 r^2 dr \quad (\text{B.1})$$

and outside of (E) the dot,

$$c_a^E = \langle \Phi_a^E | \Phi_a^E \rangle = \int d\Omega \int_R^\infty |\Phi_a^E|^2 r^2 dr \quad (\text{B.2})$$

and $c_a^I + c_a^E = 1$. Since the normalization integral of the envelope is composed of parts from the space inside and outside of the quantum dot, in the formula for the oscillator strength, we use for the γ_1 -parameter the average γ_1^R of the two values $\gamma_1^{I,E}$ of the Luttinger parameter, weighted with the normalization coefficients of the initial-state envelope:

$$\gamma_1^R = c_a^I \gamma_1^I + c_a^E \gamma_1^E. \quad (\text{B.3})$$

In the spherical approximation, $\gamma_2 = \gamma_3$, we find the oscillator strength for the dipole transition from the initial energy level E_a to the final level E_b :

$$f_{ab} = \frac{2m_0}{\hbar^2 \gamma_1^R} (E_b - E_a) \frac{1}{2F_0 + 1} \sum_{F_{0z}, F_z} |\langle \Psi_{a, F_{0z}} | z | \Phi_{b, F_z} \rangle|^2 \quad (\text{B.4})$$

with the summation over the degenerate states F_{0z} of the initial (a) = $(n_0, L_0, 3/2, F_0, F_{0z})$ level and the states F_z of the final (b) = $(n, L, 3/2, F, F_z)$ level. In a quantum dot,

$$\langle \Psi_{a, F_{0z}} | z | \Phi_{b, F_z} \rangle = \langle \Psi_{a, F_{0z}}^I | z | \Phi_{b, F_z}^I \rangle + \langle \Psi_{a, F_{0z}}^E | z | \Phi_{b, F_z}^E \rangle. \quad (\text{B.5})$$

The matrix element of $z = r n_{1(0)}$ is a product of the matrix elements of $n_{1(0)}$ and of r . The matrix elements of r are given by the integrals

$$\begin{aligned} \langle g_{a, F_{0z}} | r | f_{b, F_z} \rangle &= \langle g_{a, F_{0z}}^I | r | f_{b, F_z}^I \rangle + \langle g_{a, F_{0z}}^E | r | f_{b, F_z}^E \rangle \\ &= \int_0^R g_{a, F_{0z}}^I f_{b, F_z}^I r^3 dr + \int_R^\infty g_{a, F_{0z}}^E f_{b, F_z}^E r^3 dr. \end{aligned} \quad (\text{B.6})$$

The matrix elements of $n_{1(0)}$ can be expressed in terms of the 3- j and 6- j symbols [17] with $|L - L_0| = 1$,

$$\begin{aligned} \langle L_0, 3/2, F_0, F_{0z} | n_{1(0)} | L, 3/2, F, F_z \rangle &= \delta_{F_{0z}, F_z} [(2F_0 + 1)(2F + 1)(2L_0 + 1)(2L + 1)]^{1/2} \\ &\times (-1)^{2F - 1/2 + F_{0z}} \begin{pmatrix} F & 1 & F_0 \\ F_z & 0 & -F_{0z} \end{pmatrix} \begin{Bmatrix} L_0 & 1 & L \\ F & 3/2 & F_0 \end{Bmatrix} \begin{pmatrix} L_0 & 1 & L \\ 0 & 0 & 0 \end{pmatrix}. \end{aligned} \quad (\text{B.7})$$

The sum of the squared dipole matrix elements in equation (14) can be evaluated [37] in terms of the summation ($l_0; l$) over $(L_0, L_0 + 2; L, L + 2)$

$$\begin{aligned} &\sum_{F_{0z}, F_z} |\langle \Psi(n_0, L_0, 3/2, F_0, F_{0z}) | z | \Phi(n, L, 3/2, F, F_z) \rangle|^2 \\ &= [(2F_0 + 1)(2F + 1)/3] \left| \sum_{l_0; l} [(2l_0 + 1)(2l + 1)]^{1/2} \begin{pmatrix} l_0 & 1 & l \\ 0 & 0 & 0 \end{pmatrix} \right. \\ &\quad \left. \times \begin{Bmatrix} l_0 & 1 & l \\ F & 3/2 & F_0 \end{Bmatrix} \langle g_{n_0, l_0, F_0} | r | f_{n, l, F} \rangle \right|^2. \end{aligned} \quad (\text{B.8})$$

In particular, the $(n_0, L_0, 3/2, F_0, F_{0z}) = (1, 0, 3/2, 3/2, F_{0z})$ are the quantum numbers of the $1S_{3/2}$ ground state Γ_8 . The ground state Γ_8 will not be split by cubic terms [10] in the Hamiltonian, whereas the levels with $F > 3/2$ will be split [37]. In the semiconductor with the refractive index $n(\omega)$ at frequency ω , the linear absorption cross section [8, 14, 27, 37]

$$\sigma(\omega) = \frac{2\pi^2 e^2 \hbar}{m_0 c n(\omega)} \gamma_1^R \sum_b f_{ab} \delta(E_b - E_a - \hbar\omega) \quad (\text{B.9})$$

corresponds to transitions between the bound states a, b . Equations (14) and (B.9) with equation (B.3) apply in the general case of different values of the Luttinger parameters inside and outside of the dot.

References

- [1] Yoffe A D 1993 *Adv. Phys.* **42** 173
- [2] Nomura S, Segawa Y and Kobayashi T 1994 *Phys. Rev. B* **49** 13 571
- [3] Hatami F *et al* 1998 *Phys. Rev. B* **57** 4635
- [4] Einevoll G T and Chang Y-C 1989 *Phys. Rev. B* **40** 9683
- [5] Deng Z-Y, Guo J-K and Lai T-R 1994 *Phys. Rev. B* **50** 5736
- [6] Pasquarello A, Andreani L C and Buczko R 1989 *Phys. Rev. B* **40** 5602
- [7] Fraizzoli S, Bassani F and Buczko R 1990 *Phys. Rev. B* **41** 5096
- [8] Buczko R and Bassani F 1996 *Phys. Rev. B* **54** 2667
- [9] Baldereschi A and Lipari N O 1973 *Phys. Rev. B* **8** 2697
- [10] Baldereschi A and Lipari N O 1974 *Phys. Rev. B* **10** 1525
- [11] Xia J-B 1989 *Phys. Rev. B* **40** 8500
- [12] Sercel P C and Vahala K J 1990 *Phys. Rev. B* **42** 3690
- [13] Buczko R 1992 *Acta Phys. Pol. A* **82** 789
- [14] Buczko R and Bassani F 1992 *Phys. Rev. B* **45** 5838
- [15] Janiszewski P and Suffczyński M 1995 *Acta Phys. Pol. A* **85** 1171
- [16] Jaskólski W and Bryant G W 1998 *Phys. Rev. B* **57** R4237
- [17] Varshalovich D A, Moskalev A N, Khersonskii V K 1988 *Quantum Theory of Angular Momentum* (Singapore: World Scientific)
- [18] Pfeiffer R S and Shore H B 1982 *Phys. Rev. B* **25** 3897
- [19] Said M, Kanehisa M A, Saad Y and Balkanski M 1987 *Phys. Rev. B* **35** 687
- [20] Polupanov A F, Galiev V I and Novak M G 1997 *Fiz. Tekh. Poluprov.* **31** 1375
- [21] Bauer G E W and Ando T 1988 *Phys. Rev. B* **38** 6015
- [22] Ram-Mohan L R, Yoo K H and Aggarwal R L 1988 *Phys. Rev. B* **38** 6151
- [23] Burt M G 1992 *J. Phys.: Condens. Matter* **4** 6651
Burt M G 1993 *J. Phys.: Condens. Matter* **5** 4091
Burt M G 1995 *Semicond. Sci. Technol.* **10** 412
- [24] Foreman B A 1996 *Phys. Rev. B* **54** 1909
- [25] Goldoni C and Fasolino A 1995 *Phys. Rev. B* **51** 9903
- [26] Knipp P A and Reinecke T L 1996 *Phys. Rev. B* **54** 1880
- [27] Szmulowicz F and Brown G J 1995 *Phys. Rev. B* **51** 13 203
- [28] *Landolt-Börnstein New Series* 1982 Group III, vol 17b (Berlin: Springer)
Landolt-Börnstein New Series 1987 Group III, vol 22a (Berlin: Springer)
- [29] Yu E T, McCaldin J O and McGill T C 1992 *Solid State Physics* vol 46, ed H Ehrenreich and D Turnbull (Boston, MA: Academic) p 2
- [30] Hölscher H W, Nöthe A and Uihlein Ch 1985 *Phys. Rev. B* **31** 2379
- [31] Pelekanos N T, Ding J, Hagerott M, Nurmikko A V, Luo H, Samarth N and Furdyna J K 1992 *Phys. Rev. B* **45** 6037
- [32] Deleporte E, Lebihen T, Ohnesorge B, Roussignol Ph, Delalande C, Guha S and Munekata H 1994 *Phys. Rev. B* **50** 4514
- [33] Lee S, Michl F, Rössler U, Dobrowolska M and Furdyna J K 1998 *Phys. Rev. B* **57** 9695
- [34] Dang L S, Neu G and Romestain R 1988 *Solid State Commun.* **44** 1187
- [35] Chang S K, Nurmikko A V, Wu J-W, Kolodziejski L A and Gunshor R L 1988 *Phys. Rev. B* **37** 1191

- [36] Wasieła A, Peyla P, Merle d'Aubigné Y, Nicholls J E, Ashenford D E and Lunn B 1992 *Semicond. Sci. Technol.* **7** 571
- [37] Binnig N and Baldereschi A 1988 *Solid State Commun.* **66** 323
- [38] Leonard D, Pond K and Petroff P M 1994 *Phys. Rev. B* **50** 11 687
- [39] Bayer M, Schmidt A, Forchel A, Faller F, Reinecke T L, Knipp P A, Dremin A A and Kulakovskii V D 1995 *Phys. Rev. Lett.* **74** 3439
- [40] Bayer M, Walck S N, Reinecke T L and Forchel A 1998 *Phys. Rev. B* **57** 6584
- [41] Nair S V, Ramaniah L M and Rustagi K C 1992 *Phys. Rev. B* **45** 5969
- [42] Ramaniah L M and Nair S V 1993 *Phys. Rev. B* **47** 7132
- [43] Samuelson L and Gustafsson A 1995 *Phys. Rev. Lett.* **74** 2395
- [44] Heitz R, Veit M, Ledentsov N N, Hoffmann A, Bimberg D, Ustinov V M, Kop'ev P S and Alferov Zh I 1997 *Phys. Rev. B* **56** 10435
- [45] Heitz R, Kalburge A, Xie Q, Grundmann M, Chen P, Hoffmann A, Madhukar A and Bimberg D 1998 *Phys. Rev. B* **57** 9050
- [46] Ranjan V, Singh V A and John G C 1998 *Phys. Rev. B* **58** 1158